23rd ABCM International Congress of Mechanical Engineering
December 6-11, 2015, Rio de Janeiro, RJ, Brazil

Numerical Simulation of ONERA M6 Wing using the BRU3D CFD Code

Ricardo G. da Silva
João Luiz F. Azevedo
Edson Basso
Instituto de Aeronáutica e Espaço, DCTA/IAE/ALA, 12228-904, São José dos Campos, SP, Brazil
E-mails: *ri_galdino@yahoo.com.br*, *joaoluiz.azevedo@gmail.com*, *edsonbss@gmail.com*

Abstract.
The flow around the ONERA M6 wing, one of the most known experimental aerodynamic case, is a good test case for a code validation process, since geometry and pressure coefficient distributions at several stations along the wing are available. This test case will be used as a first step of an ongoing validation process of an in-housing this paper developed Computational Fluid Dynamics (CFD) code, named BRU3D, for aeronautic applications. Three refinement levels of a hybrid mesh composed of prism layers in a region near the wing surface, with y^+ around 1, and the rest of the domain filled by tetrahedral elements are generated. The medium mesh has roughly 6 million cells. The simulations use these meshes in conjunction with three different turbulence models, namely SA (Spalart-Allmaras) and SST (Shear Stress Transport). The comparison between pressure coefficient distributions from numerical and experimental results will give us the opportunity to find out the mesh refinement effect and the effect of turbulence models on a final solution, and hence assess discrepancies arising from such effects.

Keywords: *CFD, Turbulence Model Effects, Mesh Refinement Effects, Hybrid Meshes, Code Validation*

1. INTRODUCTION

Aerospaces and aeronautics cases usually happen at high Reynolds number and also at high Mach number, especially the aerospace applications. These types of flows are within the interests of IAE (Instituto de Aeronáutica e Espaço). Since, most of interest applications occur at high Reynolds number an adequate turbulence modelling is necessary. Moreover, flow features such as detachment due to the presence of adverse pressure gradient, interaction between shock waves and boundary layer, confluence of boundary layer and wakes, and wing tip vortex are also present in our typical flow simulation. Therefore, a successful simulation will only occur if CFD (Computational Fluid Dynamics) solver has been able to deal with such flow features.

The present work mainly focuses on aeronautics applications and all the results shown here is just a first step. Once, our final goal is to have a CFD solver that is capable of generated reliable aerodynamic results in a robust way. This achievement is possible through a process of validation and improving of the CFD solver, and at the end of this process it is possible to a solver that can be used in daily work. Therefore, the first test case selected to start the process of validation and enhancement of our in-house CFD solver (BRU3D) is Onera-M6, since its geometry and experimental data are available (Schmitt and Charpin, 1979). Moreover, this flow case presents a couple of physics features mentioned earlier, such as boundary layer/shock wave interactions and wing tip vortex, for instance.

Numerical simulation with different BRU3D settings (mesh refinement and turbulence model) of the flow around Onera-M6 wing was performed with three different mesh refinement levels, second-order spatial Roe flux-difference scheme, an implicit Euler scheme is used to march the complete set of equations, and SA and SST turbulence models. All results and comparisons between experimental data and numerical results will be presented at 4.

The present article is divided into five sections, namely Introduction, Theoretical and Numerical Formulation, Mesh, Results and Concluding Remarks. The first section, is the current section and highlight the motivations at the objective of this effort. In the fourth section, all the results obtained are presented. In the last section, conclusions and further investigations end this paper.

2. THEORETICAL AND NUMERICAL FORMULATION

In this section, not only, a brief description of a theoretical and numerical formulation. But also, a list of turbulence models and numerical schemes that are available at BRU3D will be given. This section is mainly based on Bigarella and Azevedo (2009).

The flows considered in the present paper are governed by the 3-D compressible Reynolds averaged Navier-Stokes

(RANS) equations and it is assumed to be fully turbulent. These equations in its dimensions form, are given by

$$\frac{\partial Q}{\partial t} + \nabla \cdot (E_e - E_\nu) = 0 \tag{1}$$

on which Q is given by

$$Q = [\rho \; \rho u \; \rho v \; \rho w \; \rho \tau_1 \; \rho \tau_2 \;]^T \tag{2}$$

and the inviscid (E_e) and viscous (E_ν) flux vectors are given by

$$E_e = \left\{ \begin{array}{c} \rho \mathbf{v} \\ \rho u \mathbf{v} + p\widehat{i}_x \\ \rho v \mathbf{v} + p\widehat{i}_y \\ \rho w \mathbf{v} + p\widehat{i}_z \\ (e+p)\mathbf{v} \\ \tau_1 \mathbf{v} \\ \tau 2 \mathbf{v} \end{array} \right\} \qquad E_\nu = \left\{ \begin{array}{c} 0 \\ \left(\tau^l_{xj} + \tau^t_{xj}\right)\widehat{i}_j \\ \left(\tau^l_{yj} + \tau^t_{yj}\right)\widehat{i}_j \\ \left(\tau^l_{zj} + \tau^t_{zj}\right)\widehat{i}_j \\ \beta_j \widehat{i}_j \\ \mu_{diff_1} \tau_{1,j} \widehat{i}_j \\ \mu_{diff_2} \tau_{2,j} \widehat{i}_j \end{array} \right\} \tag{3}$$

The shear-stress tensor is defined as

$$\tau^l_{ij} = \mu_l \left(\frac{\partial u_i}{\partial x_j} + \frac{\partial u_j}{\partial x_i} - \frac{2}{3} \frac{\partial u_m}{\partial x_m} \delta_{ij} \right) \tag{4}$$

on which u_I is velocity component, and x_I is referent to coordinate the system. The dynamic viscosity μ_l is determined by Sutherland law.

The unknown Favre averaged Reynolds stress tensor, τ^t , is modelled within BRU3D via linear and non-linear Eddy-Viscosity Models (EVM). The linear EVM options available in BRU3D that is going to be used in the present paper are SA turbulence model shown at Spalart and Allmaras (1994) and SST turbulence model developed by Menter (1993). The non-linear EVM is BSL-EARSM presented on Wallin and Johansson (2000) and Hellsten (2005).

The RANS equations (Eq. 1) and the turbulence model equations according to finite volume method are given by

$$V_i \frac{\partial Q_i}{\partial t} = - \sum_{k=1}^{nf} (E_{e_k} - E_{\nu_k}) \cdot S_k = -RHS \tag{5}$$

on which the subscript k stands for properties computed in the k^{th} face, and nf represents the number of faces, which form the i^{th} control volume. To obtain Eq. 5, it is assumed constant fluxes through volumes faces and also constant Q_i proprieties inside the volume faces. The first assumption is a sufficient approximation to obtaining $2nd$ order accuracy in space the currently available flux computation schemes. In the convective flux computation, a Roe flux-difference splitting scheme (Roe, 1981) is assumed. To achieve $2nd$ order accuracy in space, primitive properties are linearly reconstructed at volume faces with MUSCL algorithm (van Leer, 1979) in conjugation with limiter function, such as minmod, van Albada or super bee limiters (Hirsh, 1991) that are currently available in BRU3D. The present effort uses van Albada as limiter function. The diffusion terms are discretized using a method that computes a non oscillation, highly accurate derivatives at the face, as described in Bigarella (2007).

A $1st$-order backward Euler implicit non-linear scheme for Eq. 5 is given by

$$V_i \frac{\Delta Q^n_i}{\Delta t} = -RHS\left(Q^{n+1}_i\right) \tag{6}$$

Here, $\Delta Q^n_i = Q^{n+1}_i - Q^n_i$. The linearisation use an expansion of $RHS\left(Q^{n+1}_i\right)$ about ΔQ^n_i as in

$$RHS\left(Q^{n+1}_i\right) = RHS\left(Q^n_i\right) + \frac{\partial RHS\left(Q^n_i\right)}{\partial Q^n_i} \Delta Q^n_i + O\left(\Delta Q^n_i\right)^2 \tag{7}$$

and leads to the $1st$ order accurate implicit scheme:

$$V_i \frac{\Delta Q^n_i}{\Delta t} + \frac{\partial RHS\left(Q^n_i\right)}{\partial Q^n_i} \Delta Q^n_i = -RHS\left(Q^n_i\right) rhs \tag{8}$$

More detail in how calculate the residue $(RHS\left(Q^n_i\right))$, the Jacobian $\left[\frac{\partial RHS(Q^n_i)}{\partial Q^n_i}\right]$, and flux can be found in Bigarella and Azevedo (2009).

3. MESH

The numerical simulations will emulate a free fight condition. Hence, it is not necessary to include the wind tunnel walls in the numerical domain. However, all the experimental data were acquired from wind tunnel runs that always present wall effects. To eliminate these effects a methodology to diminish the wall effects had been applied to the experimental data. Therefore, all the comparisons, which are going to be presented in section 4, between experimental data and numerical results were done within compatible conditions.

The numerical domain consists of a semi-sphere placed at a distance equal to two hundred Mean Aerodynamic Chord (MAC) from the Onera-M6 wing surface, this quit a large distance is used to try to avoid any effect of boundaries conditions on near field flow solution. The semi-spherical outside part of the numeric domain is called Far Field and the Riemann invariants were used to impose non-reflecting boundary condition in this region. Moreover, a no slip condition imposed to the wing surface.

The mesh is divided in three levels of refinement. To generate those meshes, the number of elements inside the boundary layer is multiplied by two and size of an element that represent surface is divided by two from one refinement level to the other. It is worth to mention that all meshes are hybrids, which mean that all meshes are composed by prismatic, pyramid and tetrahedral elements. The elements attached to the wing wall surface have their Y^+ equal to 1, which gives support to solve the boundary layer without any approximation.

Figure 1 shows all three surface mesh that was generated to evaluate the mesh effect on the numerical solution. The trailing edge and wing tip has different levels of refinement when it is compared with the rest of the wing surface. At the trailing edge, this refinement is not only because of the surface curvature, but also, because it is expected a high variation of the pressure. The wing tip refinement is mainly to improve the surface and volume refinement to have a better representation of the wing tip vortex. In spite of its wing tip refinement, the fine mesh surface do not present a difference in surface mesh refinement near the wing tip. This fact occurs as a consequence of the element size set to wing surface, which is smaller than the imposed size to tip wing region.

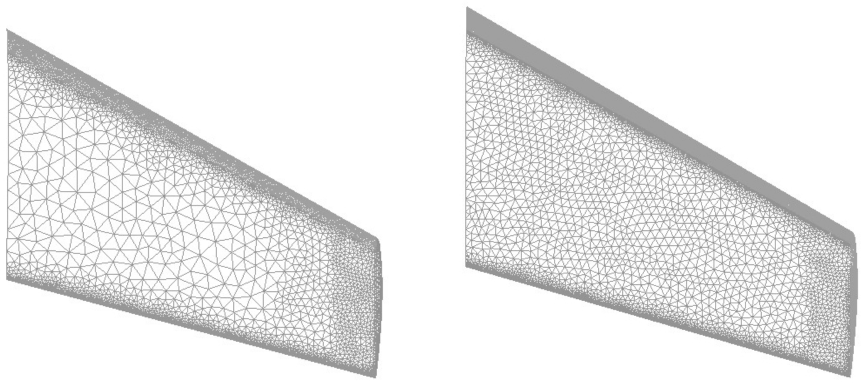

(a) Coarse Mesh (b) Baseline Mesh

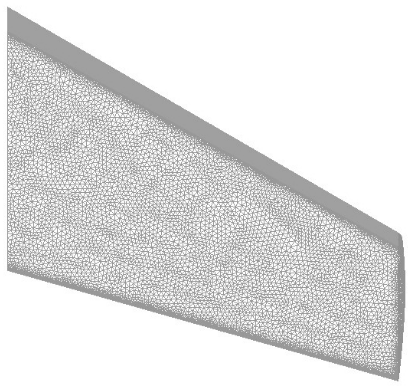

(c) Fine Mesh

Figure 1. Surface mesh according to each mesh refinement level.

Figure 2 highlights the difference on the volumetric mesh due to the refinement process. The tetrahedral growth ratio is the same for all three meshes, consequently all the volumetric refinement is directly related to the surface mesh refinement.

On the other hand, not is the prim layer height ratio identical for all meshes, once we use the number of elements inside of the prism layer as a control parameter for mesh refinement. As a consequence of these definitions, the ratio between the total number of elements for coarse mesh and for baseline mesh and the ratio total between the number of nodes for the same meshes are equal to 0.55 and 0.39, respectively. In addition, the ratio of total number of elements and total number of nodes for fine mesh in relation to baseline mesh are equal to 3.84 and 4.65, respectively. The baseline mesh has 6009711 elements and 2105122 nodes.

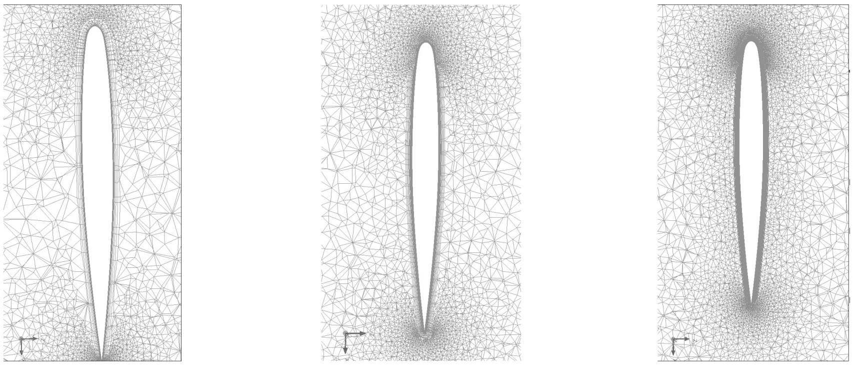

(a) Coarse Mesh (b) Baseline Mesh (c) Fine Mesh

Figure 2. Cut section of volumetric mesh localized at wing midspan position.

4. RESULTS

In this section, the numerical results obtained with BRU3D code will be compared with experimental data.The test case, as mentioned earlier, is Onera-M6 wing, which has available experimental data. For this test case, the free-stream flow conditions are Mach number equal to 0.84, Angle of Attack (AOA) of 3.06 degrees, and Reynolds number, based on MAC length, around 11.72 million. These conditions match the conditions of wind tunnel test reported in Schmitt and Charpin (1979). The experimental data correspond to pressure coefficients at seven stations along the wing span direction, each position at span-wise is shown in Tab. 1.

Table 1. The section position in which the pressure coefficient (Cp) distribution is available from wind tunnel test (Schmitt and Charpin, 1979)

Station	Relative Spanwise Position (η)	Spanwise Position (m)
S1	0.20	0.239
S2	0.44	0.526
S3	0.65	0.777
S4	0.80	0.957
S5	0.90	1.076
S6	0.95	1.136
S7	0.99	1.184

The CFL used in simulations with the coarsest mesh, baseline mesh and fine mesh was 75. The results obtained with coarse mesh in conjugation with the SA turbulence model shown that the RHS residual of mass conservation equations decreased more than 2 orders of magnitude. For baseline mesh and fine mesh with SA turbulence model, a droop on RHS residual more than 3.5 orders of magnitude was observed in the final solution. In addition, the solver setting with SST turbulence model showed a drop of more than 3.5 orders of magnitude on the residue, that was observed all mesh refinement levels. Figure 3 presents the evolution logarithm of the maximum RHS residue found in the numerical results as a function of numerical iterations. This figure shows the RHS residual for all numerical simulations that are going to be exposed in the present section.

The flow conditions, which was mentioned earlier, together with the geometry of the ONERA M6 wing are responsible for the formation of a λ shock on its upper surface. The presence of double shock wave on the suction side is typical for λ shock, on experimental data the double shock formation is present from section with $\eta = 0.20$ to section with $\eta = 0.80$. The distance between the two shock waves keeps reducing until both shocks merges into single shock, that happens somewhere between $\eta = 0.80$ and $\eta = 0.90$. All combinations of turbulence model (SA and SST) and refinement

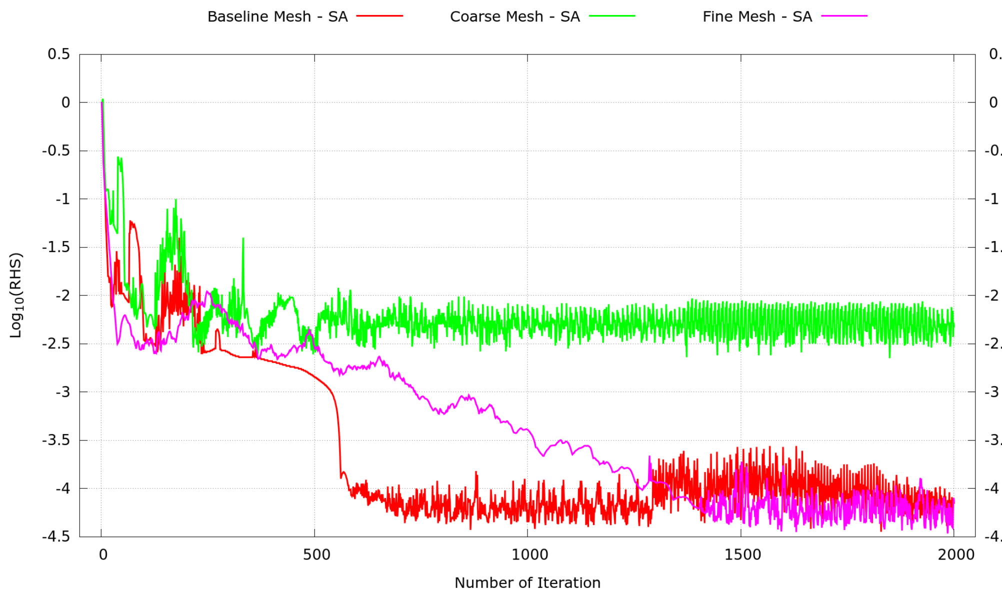

(a) SA turbulence model

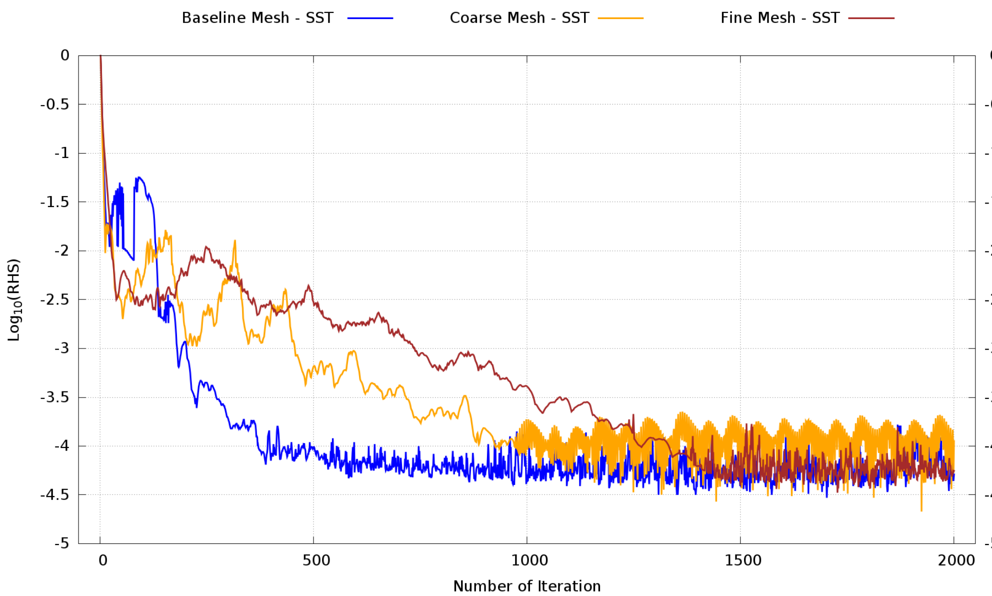

(b) SST turbulence model

Figure 3. Evolutions of RHS residue of mass conservation equation during the iteration process.

levels predicts the presence of the λ shock. However, the location where the double shocks merge is not predicted well for numerical results. The numerical results indicate the shock waves merge location somewhere between $\eta = 0.65$ and $\eta = 0.80$. Figures 4(a) and 4(b) show the Cp distribution superimposes over the Onera M6 upper surface and the isosurfaces of Mach number, respectively. The upstream isosurface is formed with Mack number equal to 1.4, and the downstream isosurface is formed with Mach number equal to 1.12. From those figures, it is noticeable the formation of the λ shock wave over the upper surface. These figures was constructed from numerical results obtained with fine mesh and SA turbulence model.

Figure 5 shows the comparison between the numerical results and experimental results of pressure distribution for the negative Cp along different spanwise locations as tabulated in Tab. 1. These comparisons in generally show good agreement between experimental data and numerical results for SA and SST turbulence in conjugation with all three mesh refinement levels.

The comparison between the numerical results obtained with SA and SST turbulence model for each mesh refinement level do not show a relevant difference from experimental data. The only exception is section $\eta = 0.20$, in which the SST turbulence model in conjugation with coarse mesh predict a different behaviour of the Cp distribution, this fact can be seen in 5(a).

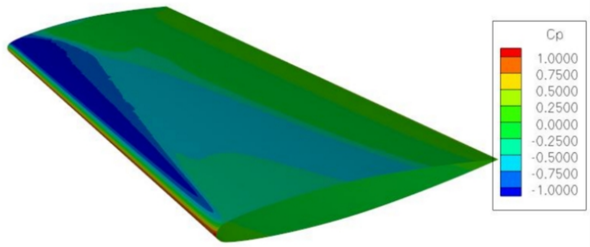

(a) Cp distribution

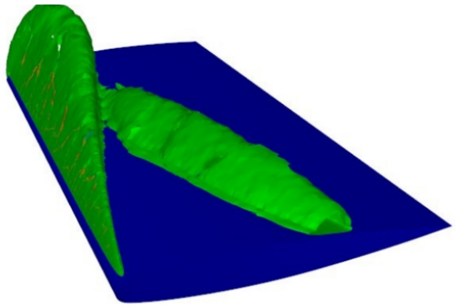

(b) Iso-surfaces of Mach number equal to 1.40 and Mach number equal to 1.12

Figure 4. Pressure coefficient distribution (Cp) and Iso-surface of Mach number equal to 1.40 and 1.12 extracted from numerical simulation obtained with fine mesh and SA turbulence model.

The mesh refinement is responsible for the major changes in the numerical results, which in general lead to diminish the discrepancy between numerical results and experimental results. The wing leading edge mesh refinement increases its local acceleration and as consequence the minimum pressure coefficient Cp decreases. The increasing on acceleration from coarse mesh to baseline mesh is bigger than the increasing from baseline mesh to fine mesh. When those mesh levels were assumed, it was thought that no difference between fine mesh results and baseline mesh results will appear. From the numerical results of both SA turbulence model and SST turbulence mode, it possible to observe a small difference between fine mesh and baseline mesh. Therefore, a further improvement on mesh refinement is still required to vanish the difference. Anyway, the mesh refinement improves the numerical results and also improves the prediction of the shock wave position, which can be seen in all figures from Fig. 5(a) to 5(c). The mesh refinement on the other sections has the same behaviour at the wing leading edge. Although, the shock position remains virtually unchanged, it can be seen in figures from Fig. 5(d) to Fig. 5(g).

As mentioned earlier, the comparison of the experimental Cp and numerical Cp shows good agreement for all spanwise sections. However, a not negligible discrepancies are found in sections $\eta = 0.20$, $\eta = 0.80$ and $\eta = 0.99$. First, the section $\eta = 0.20$ is shown in Fig. 5(a), in which there is a discrepancy between experimental and all numerical predictions for the position of the second shock wave. The mesh refinement tends to increase those discrepancies. Secondly, the section $\eta = 0.80$ is the worst result, since the double shock, which is present in experimental data, is not predicted by means of numerical simulation. None of numerical settings were able to give a corrected representation of the double shock. Finally, at section $\eta = 0.99$ (Figure 5(g)) there is a discrepancy that grows downstream from 0.60 of the local chord. The mesh refinement tends to decrease this discrepancy. Almost none effect is observed due to modifications on the turbulence model. However, both turbulence models used in the present paper were based on the same linear edge viscosity assumption. This could interpreted as indication that we are not able to predict the tip vortex with the mesh refinement levels proposed with turbulence models used.

5. CONCLUDING REMARKS

The overall behaviour of numerical results is in good agreement with experimental data, since all numerical simulations predict the formation of λ shock over the upper surface of ONERA M6, and the numerical Cp distribution present small discrepancies from experimental Cp distribution. In spite of that, the numerical results for sections $\eta = 0.20$, $\eta = 0.80$ and $\eta = 0.99$ present meaningful differences from experimental results. The difference at last section is mainly because the inefficiency in the correct prediction of the tip vortex.

None of the numerical settings (mesh refinement plus turbulence model) are able to prediction correct spanwise location of double shock merge.

To find out the causes of differences between experimental data and numerical results demands studies with respect to grid refinement, turbulence model (different models with also different assumptions) and numerical schemes. The first and second studies were done at the present article. The numerical results show no significant improvement due to modification on turbulence model, from SA to SST. However, both models are based on the same assumption for Reynolds stress, which is linear eddy viscosity. The major improvement was obtained with mesh refinement. Although the improvements on the results, a further instigation on mesh refinement is still required, since the numerical solution is still modifying from one mesh refinement level to another mesh refinement level.

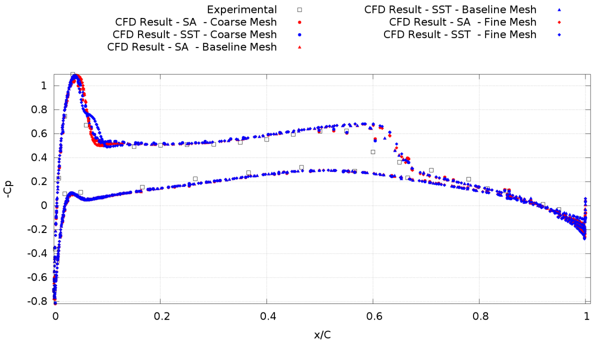

(a) $\eta = 0.20$

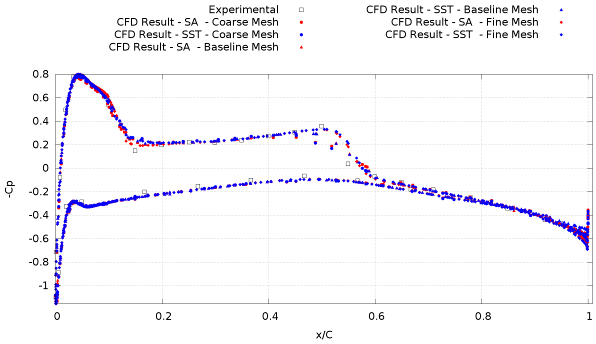

(b) $\eta = 0.44$

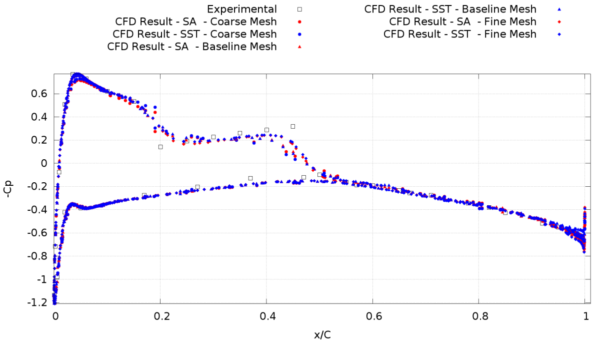

(c) $\eta = 0.65$

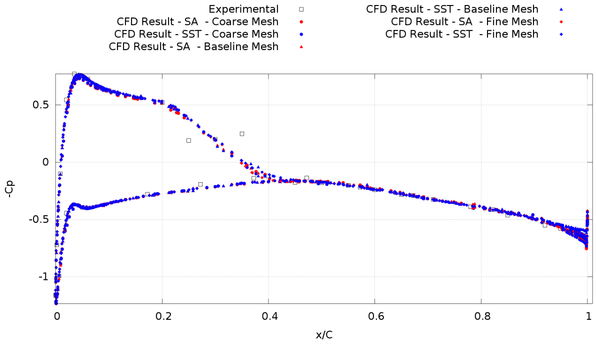

(d) $\eta = 0.80$

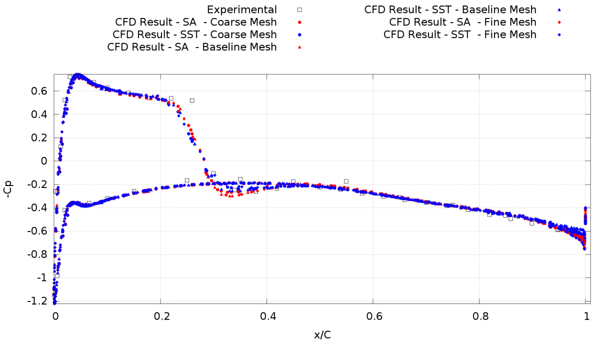

(e) $\eta = 0.90$

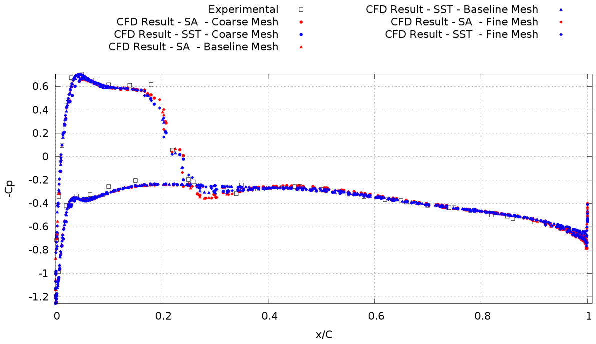

(f) $\eta = 0.95$

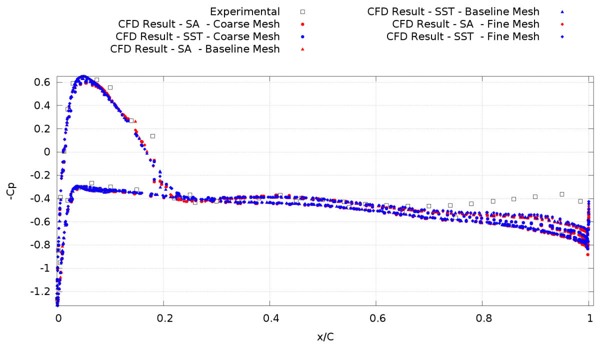

(g) $\eta = 0.99$

Figure 5. Pressure coefficient distribution along the chord for several station sections distributed along the span-wise direction. The position of each station is presented in Tab. 1.

6. ACKNOWLEDGEMENTS

The authors gratefully acknowledge the partial support for this research provided by Conselho Nacional de Desenvolvimento Científico e Tecnológico, CNPq, under the Research Grants No. 309985/2013-7, No. 400844/2014-1, No.

443839/2014-0 and No. 574004/2008-4. The authors are also indebted to the partial financial support received from Fundação de Amparo à Pesquisa do Estado de São Paulo, FAPESP, under the Research Grants No. 2008/57866-1 and No. 2013/07375-0.

7. REFERENCES

Bigarella, E. and Azevedo, J.L.F., 2009. "A unified implicit cfd approach for turbulent-flow aerospace-configuration simulations". In *Proceedings of the 47th AIAA Aerospace Sciences Meeting Including The New Horizons and Aerospace Exposition*. Orlando, USA.

Bigarella, E.D.V., 2007. *Advanced Turbulence Modelling for Complex Aerospace Applications*. Ph.D. thesis, Instituto Tecnolóco de Aeronáutica, Brazil.

Hellsten, A., 2005. "New advanced k - ω turbulence model for high-lift aerodynamics". *AIAA Journal*, Vol. 43, No. 9, pp. 1857–1869.

Hirsh, C., 1991. *Numerical Computational of Internal and External Flows*, Vol. 2. Wiley, Chichester, 1st edition.

Menter, F.R., 1993. "Zonal two equation κ - ω turbulence models for aerodynamic flows". In *24th AIAA Fluid Dynamics Conference, AIAA Paper No. 93-2906*. Orlando, USA.

Roe, P.L., 1981. "Approximate riemmann solvers, parametes vectos, and difference schemes". *Journal of Computational Physics*, Vol. 43, No. 2, pp. 357–372.

Schmitt, V. and Charpin, F., 1979. "Pressure distributions on the onera-m6-wing at transonic mach numbers". *Report of the Fluid Dynamics Panel Working Group 04, AGARD AR 138*.

Spalart, P.R. and Allmaras, S., 1994. "A one-equation turbulence model for aerodynamic flowb on a chip". *La Recherche Aeropastiale*, Vol. 1, pp. 5–21.

van Leer, B., 1979. "Towards the ultimate conservative difference scheme. v. a second-order sequel to godunovâĂŹs method". *Journal of Computational Physics*, Vol. 32, No. 2, pp. 101–136.

Wallin, S. and Johansson, A.V., 2000. "An explicit algebraic reynolds stress model for incompressible and compressible turbulent flows". *Journal of Fluid Mechanics*, Vol. 403, pp. 89–132.

8. RESPONSIBILITY NOTICE

The authors are solely responsible for the printed material included in this paper.